ChemComm

COMMUNICATION

View Article Online
View Journal | View Issue

Cite this: *Chem. Commun.*, 2020, **56**, 7869

Received 29th January 2020,
Accepted 28th February 2020

DOI: 10.1039/d0cc00279h

rsc.li/chemcomm

Cross-β amyloid nanotubes for hydrolase–peroxidase cascade reactions†

Ayan Chatterjee, Syed Pavel Afrose, Sahnawaz Ahmed, Akhil Venugopal and Dibyendu Das *

Herein, we report the catalytic potential of short peptide based cross-β amyloid nanotubes with surface exposed histidine capable of binding hemin and showing facile cascade reactions, playing the dual roles of hydrolases and peroxidases, two of the most important classes of enzymes in extant biology. The activity of these simple systems exceeded those of modern and larger proteins like cytochrome *C* and hemoglobin. Further, evidence suggested that these self-assembled nanotubes foreshadow the process of intermediate channeling, a feature seen in the case of advanced enzymes.

Millions of years ago, inside Darwin's warm pond rich in nutrients, the origins of chemical evolution demanded the presence of a diverse chemical inventory and chemical networks.[1,2] Computer simulation studies of these networks have argued for reaction diffusion models and supported the notion of diffusion differences to channel reaction substrates.[3] Reactions such as oxidation of fuels achieved through a sequence of cascade reactions must have helped in the emergence of more complex products from simple precursors, thus enriching the inventory further.[1–3] These chemical networks could indeed become mutually connected, eventually leading to stochastic innovation, best exemplified in Darwinian evolution.[2] Chemical gradients and diffusion differences of reaction substrates are exploited in extant biology to master the art of single pot reactions in metabolic pathways. Enzymatic cascade reactions are carried out using proximally aligned biocatalysts where non-covalent associations and spatial co-localizations allow the product of one enzyme to act as a substrate for the other in the complex.[3] Hence, this intermediate can channel to the adjacent active sites, resulting in enhancement of rates. This process is known as substrate channeling, which is advantageous in the context of minimizing, if not completely removing the expenses of reaching equilibrium with the bulk.

We asked whether a minimal system based on short peptide based assemblies can show cascade catalysis and benefit from such channeling as observed in modern enzymes.[4–8] Many research laboratories including ours have reported the remarkable binding capabilities of short amyloid-forming peptides for diverse guests.[4–13] Amyloid peptides and their assembly under prebiotic conditions have been shown recently by Riek and coworkers.[1e,h,i] Amyloid assemblies have also been elegantly scored for enzyme like activities and the results argue the evolution of enzymes from short assembling folds.[14,15] We propose that exposed arrays of active site residues of amyloid assemblies coupled with their binding capabilities to attract co-factors/prosthetic groups can help amyloid to perform catalytic roles of multiple enzymes. Further, binding surfaces enriched with catalytic sites might promote channeling of cascade intermediates among the proximal sites (Fig. 1).

We used a short peptide fragment (^{17}LVFFA^{21}) from the nucleating core of an Aβ (1–42) amyloid, an extensively studied sequence seen in the fibrillar deposits of Alzheimer's disease.[4–12] This pentapeptide is known to access distinct morphologies with acute responsiveness to environmental switches.[5–8,9a] Ac-**H**LVFFA**L**-$CONH_2$ (**HL**) was synthesized which assembles to form homogenous nanotubes with diameters of 35 ± 4 nm at pH 3 (Fig. 1a and c; Fig. S1–S3, ESI†). To investigate the exposure of histidines on their surfaces, the assemblies were incubated with negatively charged gold nanoparticles (Neg-AuNPs, Fig. 2 and Fig. S4, ESI;† for details of the pH effects on binding see Fig. S5A, ESI†). Homogenous tubular morphologies of similar dimensions with ordered arrays of AuNPs were observed under TEM and SEM (Fig. 2a–c, ESI†). A control experiment with cationic AuNPs did not yield any specific binding (Fig. S5B, ESI†), thus suggesting the presence of surface exposed histidines.

To probe the binding capability of these nanotubes, the hydrophobic fluorescent dye coumarin 343 was used as a model guest. Under a confocal fluorescence microscope (CLSM), fluorescent tubular structures were observed (Fig. 2d, controls in Fig. S6, ESI†). Blue shift in absorbance spectra was also observed upon binding (Fig. S7, ESI†). We expected that the nanotubes should also bind other small molecules like hemin – the prosthetic group of peroxidases and many metalloproteins. To create

Department of Chemical Sciences and Centre for Advanced Functional Materials, Indian Institute of Science Education and Research (IISER) Kolkata, Mohanpur-741246, India. E-mail: dasd@iiserkol.ac.in

† Electronic supplementary information (ESI) available. See DOI: 10.1039/d0cc00279h

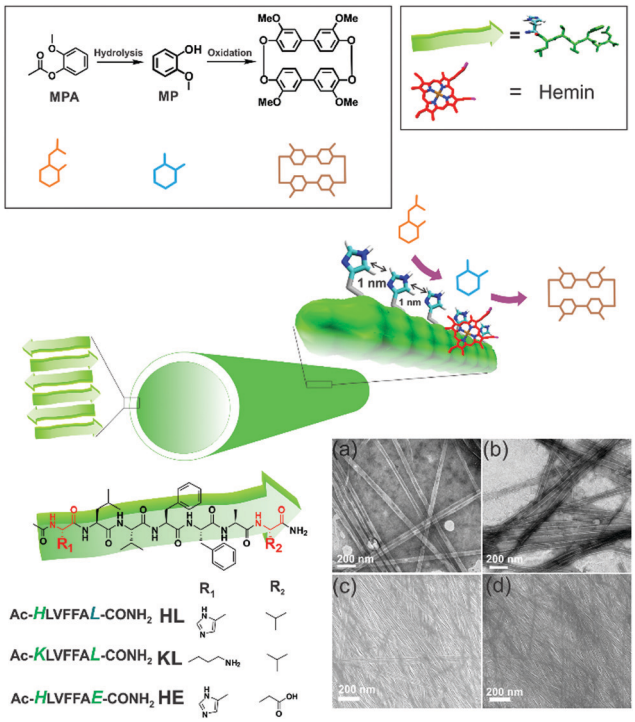

Fig. 1 Scheme showing cascade reaction on nanotube surface, and chemical structures of amyloid, MPA, MP and the oxidation product. TEM and SEM images of self-assembled **HL** (a and c) and **KL** (b and d) respectively.

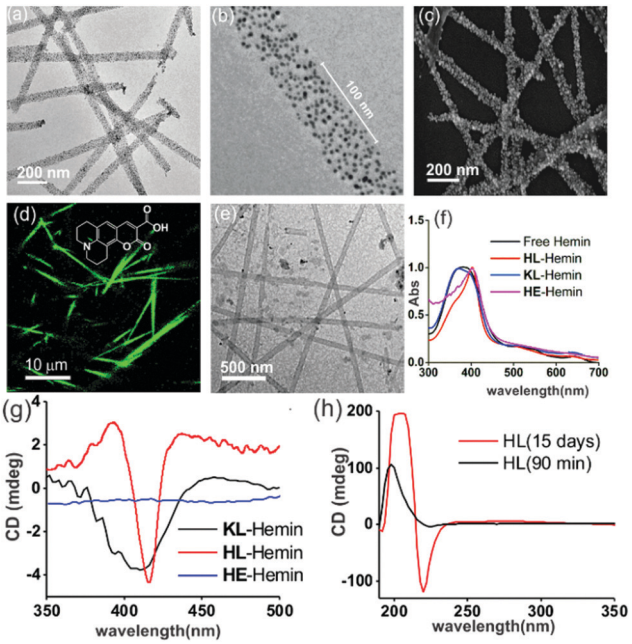

Fig. 2 (a) TEM image of negative-AuNPs bound with **HL** and (b) an enlarged TEM image of a negative-AuNP bound with **HL**. (c) SEM image of AuNP–**HL** nanotubes. (d) CLSM image (λ_{ex} = 488 nm) of Coumarin 343 dye bound to **HL**. (e) TEM image of hemin–**HL**. (f) Normalized UV-Vis spectra of free hemin, and hemin in the presence of **HL**, **KL**, and **HE** at pH 3. (g) CD spectra of hemin bound **HL**, **KL**, and **HE**. (h) CD spectra of HFIP treated **HL** after 90 min and 15 days.

hemin bound assemblies, varying concentrations of hemin were mixed with 1 mM **HL**. The mole ratio varied in the range of *ca.* 1 : 150 of hemin : peptide with half of the peptide buried in the bilayer structure (Fig. S8A, ESI†).[6] TEM showed no change in **HL** morphology after interaction with hemin (Fig. 2e). UV-Vis spectra show that unbound hemin had a Soret peak at 395 nm at pH 3 with a lower intensity peak at 365 nm, which is similar to the spectrum observed in water (Fig. S9, ESI†).[16,17] These two major peaks suggested the presence of a dimer of hemin (μ-oxo bihemin) along with hemin-hydroxide (haematin) respectively. The 640 nm peak suggested the Q band value of the dimer.[16a,17] In the presence of **HL** (pH 3), the Soret band of bound hemin significantly shifted to 404 nm with a shoulder of the hemin at 365 nm. The red shifted Soret peak suggested the formation of a hemin–histidine complex and lesser extent of hemin aggregation.[16a,17] Circular dichroism (CD) showed an induced negative Cotton effect due to the achiral hemin, thus suggesting binding to the chiral surface of the nanotube (Fig. 2g). However, a crossover point at 404 nm suggested exciton coupling and hence indicated some dimerization.[17b] The peroxidase-like activity of these hemin–**HL** assemblies was then investigated. We used 2-methoxy phenol (MP, Fig. 1), a widely used substrate for monitoring peroxidase activity. Hemin–**HL** showed peroxidase like activity with k_c = 14.5 ± 0.9 min^{-1} (Table S1; Fig. S10, ESI;† kinetic measurements were done at a fixed H_2O_2 concentration (30 mM); Fig. S11 (ESI†) for the effect of H_2O_2 concentration on the oxidation of MP).

For tandem catalysis, the substrate undergoes consecutive reactions without the need for isolation of intermediates. Hence, MP was acetylated to form 2-methoxy phenyl acetate (MPA, Fig. 1) with the expectation that the hemin–**HL** nanotubes will first hydrolyze the ester to create the intermediate phenol MP which can be subsequently oxidized. The rate of oxidation will imply the rate of the tandem reaction. When hemin (0.01 mM) bound **HL** nanotubes were used for the acetylated phenol (MPA), rapid oxidation was observed (k_c = 7.7 ± 0.7 min^{-1}, Fig. 3a; see the ESI† for detailed kinetic treatment; Fig. S12 and Table S1; and see Fig. S13 (ESI†) for the effect of H_2O_2 concentration on the oxidation of MPA) at pH 3.[18] From the pH rate profile, **HL**–hemin showed the highest activity at pH 3 (Fig. S11, ESI†). The reason for this could be attributed to the bundling of the **HL** nanotubes at higher pH as observed in TEM and scattering experiments (Fig. S14, ESI†). Varying hemin concentrations showed the highest activity at 0.01 mM hemin (Fig. S8B, ESI†). For controls, first Ac-**K**LVFFA**L**-$CONH_2$ (**KL**, Fig. 1 and Fig. S15, ESI†) was synthesized.[5–7,14a] **KL** formed morphologically indistinguishable nanotubes (diameters of 36 ± 4 nm, Fig. 1b and d) and bound to Neg-AuNPs in a similar fashion to **HL**, suggesting the exposure of lysines on its nanosurface (Fig. S16, ESI†). Also, hemin binding was indicated by CD and UV-Vis spectra (Fig. 2f and g). Hemin bound lysine nanotubes showed low peroxidase activity with MP (k_c = 0.5 ± 0.03 min^{-1} at pH 3, Table S1, ESI†) but substantially higher activity in the presence of histidine (1 mM, k_c = 11.5 ± 0.8 min^{-1}) as histidine is known to augment hemin activity (Table S1, ESI†).[16a] However, when the tandem reaction was monitored with acetylated phenol MPA as a substrate, hemin–**KL** nanotubes showed meagre activity of

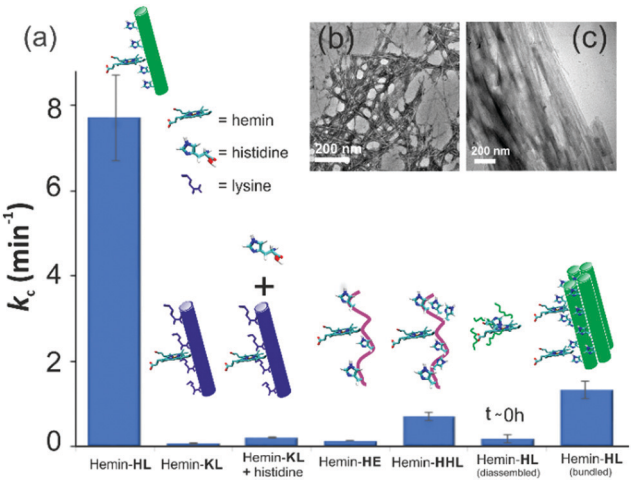

Fig. 3 (a) Tandem activity with MPA. TEM images of (b) **HE** nanofibers and (c) bundled **HL**. [Hemin] = 0.01 mM, [peptide] = 1 mM, [H_2O_2] = 30 mM, [MPA] = 5 to 30 mM. Results are reported in triplicates.

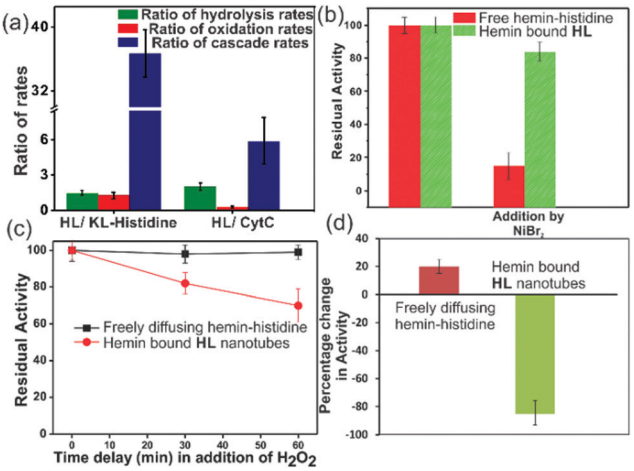

Fig. 4 (a) Ratios of the rates of **HL** to **KL**–histidine systems and **HL** to Cyt*C* for hydrolysis, oxidation and cascade reactions. Residual activities of (b) free hemin–histidine and hemin–HL systems challenged by inhibitor $NiBr_2$, (c) delayed addition of H_2O_2 to the free histidine hemin and hemin–HL systems, (d) percentage change in activity when MPA was added to **HL** or only histidine without hemin, and after 10 min delay, hemin was added. [Hemin] = 0.01 mM, [**HL**] = 1 mM, [histidine] = 1 mM, [H_2O_2] = 30 mM.

0.08 ± 0.01 min^{-1} (Fig. 3 and Table S1, ESI†). Addition of 1 mM histidine to hemin–**KL** did not result in any notable increase of activity (k_c = 0.21 ± 0.02 min^{-1}, Table S1 and Fig. S17, ESI†). This significant decrease of *ca.* 37 fold in hemin–**KL**–histidine with respect to hemin–**HL** underpinned the importance of exposed histidines for tandem catalysis. Notably, despite the similar oxidation rates for MP by the hemin–**HL** and hemin–**KL**–histidine systems, the substantially lower rates for the tandem reaction suggest the importance of the hydrolysis step in the cascade process. Extant proteins like cytochrome *C* (Cyt*C*) and hemoglobin (Hb) showed high peroxidase activity with MP with k_c values of 49.1 ± 5.3 min^{-1} and 12 ± 1.3 min^{-1}. However, with MPA as a substrate, both proteins showed substantially decreased tandem rates of k_c = 1.13 ± 0.09 min^{-1} and 0.84 ± 0.01 min^{-1}, respectively, despite the presence of multiple histidines in their respective sequences. Remarkably, this hemin-short peptide-based system had 6.8 fold higher cascade activity than Cyt*C*, despite the oxidation rate being more than 3 times lower (Fig. 4a).

To check the role of morphologies, we disassembled **HL** nanotubes with hexafluoroisopropanol (HFIP) as monitored from the loss of CD signals and TEM structures (Fig. 2h and Fig. S18, ESI†). With these disassembled **HL** nanotubes, hemin showed similar UV-Vis spectra to that observed for unbound hemin (Fig. S19, ESI†). The disassembled system showed 40 times lower activity (Fig. 3a). The terminal leucine of **HL** was mutated to form Ac-**H**LVFFA**E**-CONH$_2$ (**HE**) which assembled to form nanofibers having diameters of 11 ± 2 nm (Fig. 3b and Fig. S20 and S21, ESI†). Hemin–**HE** showed a Soret peak at 404 nm, indicating histidine–hemin interaction, while CD did not show any induced peak (Fig. 2f and g). Hemin–**HE** showed decent peroxidase activity with MP (k_c of 7.22 ± 0.65 min^{-1}, Table S1, ESI†) but the tandem activity with MPA was substantially lower (k_c = 0.14 ± 0.01 min^{-1}, Fig. 3a and Table S1, ESI†). Addition of one more histidine residue at the N-terminus (Ac-**HH**LVFFA**L**-CONH$_2$, **HHL**) resulted in nanofibrillar assembly (Fig. S22 and S23, ESI†) but still had 11 fold lower activity than **HL** (Fig. 3a and Table S1, ESI†). This result suggested the importance of a nanotubular morphology for cascade catalysis. To further investigate the role of nanosurfaces, Na_2SO_4 was added to induce bundling of nanotubes where the activity decreased to 1.32 ± 0.12 min^{-1} (Fig. 3c).[5,6] Control experiments performed with free hemin–histidine systems in the presence of sodium sulfate did not show any decrease of activity, thus underpinning the role of the nanotubes for efficient cascade.

To probe the substantially faster cascade rates observed in the case of **HL** over the **KL**–histidine system (*ca.* 38 fold) and even enzymes such as Cyt*C* (*ca.* 6.8 fold), we compared the rates for hydrolysis reaction of MPA (Fig. 4a and Fig. S24–S26, ESI†). Interestingly, the ratios of the hydrolysis rates of **HL** to **KL**–histidine and Cyt*C* were found to be moderate (1.3 and 2 fold respectively). Hence, the reason for this significantly higher activation for cascade could be due to channeling in the histidine exposed **HL** nanotubes. To probe channeling, the cascade reaction was challenged by a reaction in the bulk environment.[3] This method involved the addition of an inhibitor for the oxidation step (Fig. 4b).[19] If intermediate channeling occurs, hemin–**HL** will show a lesser extent of inhibition compared to a reaction which happens in a freely diffusing bulk state. We used a combination of unbound hemin and free histidine as our freely diffusing model system which showed low but measurable rates with MPA (1.35 ± 0.11 min^{-1}, Fig. S27, ESI†) only at higher pH 8, due to the nucleophilic hydrolytic and intrinsic peroxidase activities of histidine and hemin respectively.[17d] Ni^{2+} ions, a known inhibitor for the oxidation step of peroxidases, were added as a premixed solution with H_2O_2 to both the freely diffusing and hemin–**HL** systems.[19] In the case of MP, the residual activity slumped down to almost 50% and 30% for the **HL**–hemin and freely diffusing systems, respectively (Fig. S28, ESI†), whereas for the

cascade reaction with MPA, the activity of the freely diffusing system plummeted to 15% of the initial activity (Fig. 4b). However, for MPA with hemin–**HL**, the residual activity was still 85%, suggesting channeling in the nanotubes (Fig. 4b). Since H_2O_2 oxidizes MP, in a separate experiment we delayed H_2O_2 addition to allow the leakage of intermediate phenol, which is the substrate for hemin and hence would impede channeling. For the bulk, delayed addition of H_2O_2 did not have any effect on the tandem activity (Fig. 4c). Interestingly, for hemin–**HL**, the activity decreased significantly with time, suggesting the leakage of the cascade intermediate MP after hydrolysis (Fig. 4c). To investigate further, we induced the leakage of the intermediate by also delaying the association between hemin and **HL**. For this purpose, we added the substrate MPA to nanotubes without hemin, and after *ca.* 10 min delay for leaking, we added hemin. The cascade activity for this system decreased to 12 fold. However, a similar experiment with the freely diffusing system registered a slight increase in activity (Fig. 4d).

In summary, we have reported a short peptide-based amyloid with arrays of active site residues capable of binding prosthetic groups and displaying the catalytic potential of cascade reactions. With distances of *ca.* 1 nm between the residues,[6] these peptide based short amyloid assemblies foreshadow the concept of intermediate channeling, which is observed in modern enzyme complexes. The system has some limitations in terms of pH. Current efforts are intended to develop systems with a greater substrate scope and higher pH tolerance.

DD is thankful to a Nanomission Grant (SR/NM/NS-1082/2015), DST, GOI, AC acknowledges CSIR, SPA acknowledges UGC and SA acknowledges NPDF (PDF/2017/000782), SERB.

Conflicts of interest

The authors declare no conflicts of interest.

Notes and references

1 (*a*) C. R. Woese, *Proc. Natl. Acad. Sci. U. S. A.*, 2002, **99**, 8742–8747; (*b*) J. Greenwald and R. Riek, *J. Mol. Biol.*, 2012, **421**, 417–426; (*c*) O. Carny and E. Gazit, *FASEB J.*, 2005, **19**, 1051–1055; (*d*) J. T. Goodwin, A. K. Mehta and D. G. Lynn, *Acc. Chem. Res.*, 2012, **45**, 2189–2199; (*e*) J. Greenwald, M. P. Friedmann and R. Riek, *Angew. Chem., Int. Ed.*, 2016, **55**, 11609–11613; (*f*) C. P. Maury, *Origins Life Evol. Biospheres*, 2009, **39**, 141–150; (*g*) B. M. Rode, *Peptides*, 1999, **20**, 773–786; (*h*) J. Greenwald, W. Kwiatkowski and R. Riek, *J. Mol. Biol.*, 2018, **430**, 3735–3750; (*i*) S. K. Rout, M. P. Friedmann, R. Riek and J. Greenwald, *Nat. Commun.*, 2018, **9**, 234; (*j*) J. E. Smith, A. K. Mowles, A. K. Mehta and D. G. Lynn, *Life*, 2014, **4**, 887–902.

2 J. A. Bradford and K. A. Dill, *Proc. Natl. Acad. Sci. U. S. A.*, 2007, **104**, 10098–10103.

3 (*a*) I. Wheeldon, S. D. Minteer, S. Banta, S. C. Barton, P. Atanassov and M. Sigman, *Nat. Chem.*, 2016, **8**, 299–309; (*b*) Y. Gao, C. C. Roberts, J. Zhu, J.-L. Lin, C. A. Chang and I. Wheeldon, *ACS Catal.*, 2014, **5**, 2149–2153; (*c*) Y. Zhang, S. Tsitkov and H. Hess, *Nat. Catal.*, 2018, **1**, 276–281; (*d*) X. Zhao, H. Palacci, V. Yadav, M. M. Spiering, M. K. Gilson, P. J. Butler, H. Hess, S. J. Benkovic and A. Sen, *Nat. Chem.*, 2018, **10**, 311–317; (*e*) R. Guha, F. Mohajerani, M. Collins, S. Ghosh, A. Sen and D. Velegol, *J. Am. Chem. Soc.*, 2017, **139**, 15588–15591.

4 G. Wei, Z. Su, N. P. Reynolds, P. Arosio, I. W. Hamley, E. Gazit and R. Mezzenga, *Chem. Soc. Rev.*, 2017, **46**, 4661–4708.

5 N. Kapil, A. Singh and D. Das, *Angew. Chem., Int. Ed.*, 2015, **54**, 6492–6495.

6 W. S. Childers, A. K. Mehta, R. Ni, J. V. Taylor and D. G. Lynn, *Angew. Chem., Int. Ed.*, 2010, **49**, 4104–4107.

7 N. Kapil, A. Singh, M. Singh and D. Das, *Angew. Chem., Int. Ed.*, 2016, **55**, 7772–7776.

8 S. Li, A. N. Sidorov, A. K. Mehta, A. J. Bisignano, D. Das, W. S. Childers, E. Schuler, Z. Jiang, T. M. Orlando, K. Berland and D. G. Lynn, *Biochemistry*, 2014, **53**, 4225–4227.

9 (*a*) A. Singh, N. Kapil, M. Yenuganti and D. Das, *Chem. Commun.*, 2016, **52**, 14043–14046; (*b*) B. G. Cousins, A. K. Das, R. Sharma, Y. Li, J. P. McNamara, I. H. Hillier, I. A. Kinloch and R. V. Ulijn, *Small*, 2009, **5**, 587–590.

10 (*a*) T. P. J. Knowles and R. Mezzenga, *Adv. Matter*, 2016, **28**, 6546–6561; (*b*) A. J. Baldwin, T. P. J. Knowles, G. G. Tartaglia, A. W. Fitzpatrick, G. L. Devlin, S. L. Shammas, C. A. Waudby, M. F. Mossuto, S. Meehan, S. L. Gras, J. Christodoulou, S. J. Anthony-Cahill, P. D. Barker, M. Vendruscolo and C. M. Dobson, *J. Am. Chem. Soc.*, 2011, **133**, 14160–14163; (*c*) M. R. Elkins, T. Wang, M. Nick, H. Jo, T. Lemmin, S. B. Prusiner, W. F. DeGrado, J. Stöhr and M. Hong, *J. Am. Chem. Soc.*, 2016, **138**, 9840–9852.

11 (*a*) T. P. Knowles, A. W. Fitzpatrick, S. Meehan, H. R. Mott, M. Vendruscolo, C. M. Dobson and M. E. Welland, *Science*, 2007, **318**, 1900–1903; (*b*) J. Kaplanm and W. F. DeGrado, *Proc. Natl. Acad. Sci. U. S. A.*, 2004, **101**, 11566–11570; (*c*) C. B. Bell, J. R. Calhoun, E. Bobyr, P.-P. Wei, B. Hedman, K. O. Hodgson, W. F. DeGrado and E. I. Solomon, *Biochemistry*, 2009, **48**, 59–73.

12 (*a*) C. M. Micklitsch, P. J. Knerr, M. C. Branco, R. Nagarkar, D. J. Pochan and J. P. Schneider, *Angew. Chem., Int. Ed.*, 2011, **50**, 1577–1579; (*b*) M. P. Hendricks, K. Sato, L. C. Palmer and S. I. Stupp, *Acc. Chem. Res.*, 2017, **50**, 2440–2448; (*c*) R. Freeman, M. Han, Z. Álvarez, J. A. Lewis, J. R. Wester, N. Stephanopoulos, M. T. McClendon, C. Lynsky, J. M. Godbe, H. Sangji, E. Luijten and S. I. Stupp, *Science*, 2018, **362**, 808–813.

13 Y. Gao, F. Zhao, Q. Wang, Y. Zhang and B. Xu, *Chem. Soc. Rev.*, 2010, **39**, 3425–3433.

14 (*a*) T. O. Omosun, M.-C. Hsieh, W. S. Childers, D. Das, A. K. Mehta, N. R. Anthony, T. Pan, M. A. Grover, K. M. Berland and D. G. Lynn, *Nat. Chem.*, 2017, **9**, 805–809; (*b*) C. Zhang, R. Shafi, A. Lampel, D. MacPherson, C. Pappas, V. Narang, T. Wang, C. Madarelli and R. V. Ulijn, *Angew. Chem., Int. Ed.*, 2017, **56**, 14511–14515; (*c*) C. M. Rufo, Y. S. Moroz, O. V. Moroz, J. Stöhr, T. A. Smith, X. Hu, W. F. DeGrado and I. V. Korendovych, *Nat. Chem.*, 2014, **6**, 303–309; (*d*) C. Zhang, X. Xue, Q. Luo, Y. Li, K. Yang, X. Zhuang, Y. Jiang, J. Zhang, J. Liu, G. Zou and X. J. Liang, *ACS Nano*, 2014, **8**, 11715–11723.

15 (*a*) M. O. Guler and S. I. Stupp, *J. Am. Chem. Soc.*, 2007, **129**, 12082–12083; (*b*) N. Singh, M. Kumar, J. F. Miravet, R. V. Ulijn and B. Escuder, *Chem. – Eur. J.*, 2017, **23**, 981–993; (*c*) J. Meeuwissen and J. N. H. Reek, *Nat. Chem.*, 2010, **2**, 615–621.

16 (*a*) Q. Wang, Z. Yang, X. Zhang, X. Xiao, C. K. Chang and B. Xu, *Angew. Chem., Int. Ed.*, 2007, **46**, 4285–4289; (*b*) Q. G. Wang, Z. M. Yang, L. Wang, M. Ma and B. Xu, *Chem. Commun.*, 2007, 1032–1034; (*c*) Q. Wang, L. Li and B. Xu, *Chem. – Eur. J.*, 2009, **15**, 3168–3172.

17 (*a*) P. K. Shantha, G. S. S. Saini, H. H. Thanga and A. L. Verma, *J. Raman Spectrosc.*, 2001, **32**, 159; (*b*) S. Matile, N. Berova, K. Nakanishi, J. Fleischhauer and R. W. Woody, *J. Am. Chem. Soc.*, 1996, **118**, 5198–5206; (*c*) G. J. Corban, S. K. Hadjikakou, A. C. Tsipis, M. Kubicki, T. Bakas and N. Had- jiliadis, *New J. Chem.*, 2011, **35**, 213–224; (*d*) T. Uno, A. Takeda and S. Shimabayashi, *Inorg. Chem.*, 1995, **34**, 1599–1607.

18 K. J. Laidler, *Chemical Kinetics*, Pearson Education, New Delhi, 1987.

19 F. Pintus, A. Mura, A. Bellelli, A. Arcovito, D. Spanò, A. Pintus, G. Floris and R. Medda, *FASEB J.*, 2008, **275**, 1201–1212.

